AC susceptibility studies of magnetic relaxation in nanoparticles of Ni dispersed in silica

V. Singh and M. S. Seehra*

Department of Physics, West Virginia University, Morgantown, WV 26506, USA

J. Bonevich

National Institute of Standards and Technology, Gaithersburg, MD 20899, USA

Abstract

Temperature dependence of AC susceptibilities χ' and χ'' are reported using frequencies f_m = 0.1 Hz, 1 Hz, 99 Hz, 499 Hz and 997 Hz for nanoparticles (NPs) of Ni dispersed in silica (Ni/SiO_2:15/85) with the mean sizes D=3.8 nm, 11.7 nm, 15 nm and 21nm. ($\sigma \simeq 0.2$nm), as determined by TEM. The blocking temperatures T_B, as determined by peaks in χ'' vs. T data, are fit to the Vogel-Fulcher law based Eq.: $T_B = T_o + T_a/\ln(f_o/f_m)$ with the attempt frequency $f_o = 2.6\times10^{10}$ Hz and $T_a(T_o)$ = 320(0) K, 990(0) K, 1370(6) K and 1500(9) K for D = 3.8 nm, 11.7 nm, 15 nm and 21nm, respectively. These magnitudes of $T_a = K_a V/k$ yield the anisotropy constant K_a increasing with decreasing D (or volume V) due to contributions from surface anisotropy. The validity of the theoretical result $\chi'' = C\partial(\chi' T)/\partial T$ with $C \simeq \pi/[2\ln(f_o/2\pi f_m)]$ is checked. The non-zero but small magnitudes of T_o for the two larger particles suggest the presence of very weak interparticle interaction.

*Author to whom correspondence should be addressed. Electronic mail: mseehra@wvu.edu

INTRODUCTION

Among several factors that affect the measured properties of magnetic nanoparticles (NPs) include size and size distribution, magnetic field H, temperature T, interparticle interactions, and the time scale or frequency f_m of measurements [1,2]. The intrinsic anisotropy K_a which is often size-dependent due to different contributions from bulk anisotropy K_b and surface anisotropy K_s also has major effect on the observed magnetic properties [3-6]. In this work, we report our investigations of the magnetic relaxation of Ni NPs dispersed in silica with average particle diameters D=3.8 nm, 11.7 nm, 15 nm and 21nm by measuring the temperature dependence of the AC susceptibilities χ' and χ'' at f_m=0.1 Hz, 1 Hz, 99 Hz, 499 Hz and 997 Hz. The particles were synthesized via the citric acid sol-gel route with the Ni:SiO_2 composition of 15:85 [7] in order to increase the interparticle separation and hence reduce the interparticle interaction. For non-interacting NPs subjected to a slowly oscillating magnetic field $h=h_o cos\omega_m t$, χ' and χ'' are given by [2,8]:

$$\chi' = \chi_o / [1+(\omega_m\tau)^2] \quad (1)$$

$$\chi'' = \chi_o\omega_m\tau / [1+(\omega_m\tau)^2] \quad (2)$$

where the relaxation frequency $f=1/\tau$ is given [1,2]:

$$f = f_o exp(-T_a/T) \quad (3).$$

Here $T_a=K_aV/k$ for a particle of volume V with k being the Boltzmann constant, χ_o is the static susceptibility for $\omega \rightarrow 0$, $\omega_m=2\pi f_m$ and f_o is the attempt frequency. For random orientation of the easy axis of the particles each with magnetic moment $\mu=M_sV$, χ' and χ'' of Eq. (1) and (2) can be written as [8]:

$$\chi' = (M_s^2/3K_a)[1+(T_a/T)(1/(1+(\omega_m\tau)^2))] \quad (4)$$

$$\chi'' = (M_s^2/3K_a)[(T_a/T)(\omega_m\tau/(1+(\omega_m\tau)^2))] \quad (5).$$

The blocking temperature T_B of the particles is determined from Eq. (3) for $f=f_m$ yielding

$$T_B=T_a/\ln(f_o/f_m) \qquad (6).$$

In the presence of weak interparticle interaction (IPI), Eq (6) is replaced by Eq. (7) below, derived from the Vogel-Fulcher law [9-11]:

$$TB=T_o+T_a/\ln(f_o/f_m) \qquad (7)$$

where T_o measures the strength of IPI. According to Eqs. (6) and (7), T_B increases with increase in f_m. Also from the above equations, it can be shown that χ'' is maximum at $\omega_m\tau=1$ and χ' and χ'' are related by [2]:

$$\chi''=C\partial(\chi'T)/\partial T \text{ where } C\simeq\pi/[2\ln(f_o/2\pi f_m)] \qquad (8).$$

In this work, the above equations are used to interpret the frequency dependence of χ' and χ'' and determine T_B, f_o and T_a, the latter leading to the variation of the anisotropy constant K_a as size of the Ni NPs is varied. We also check the validity of Eq. (8).

EXPERIMENTAL RESULTS AND DISCUSSION

The NPs of Ni/SiO_2 (15/85) were synthesized following the procedure outlines in an earlier paper [7]. Annealing the samples at 400 ^oC, 500 ^oC, 600 ^oC and 700^oC for 2 hours in ultra high pure N_2 gas produced particles of average size D=3.8(0.2) nm, 11.7(0.2) nm, 15(0.2) nm and 21(0.12) nm as determined by TEM (Transmission Electron Microscopy). In Fig. 1, we show the representative TEM for 21 nm NPs with log-normal fit to the histogram of the particle sizes. The corresponding x-ray diffraction (XRD) patterns for all four sizes using CuK_α source (λ=0.154185 nm) are shown in Fig. 2. No lines other than those of Ni and amorphous SiO_2 ($2\theta\cong22^o$) are observed. The sizes determined from XRD are consistent with those determined from TEM. Measurements of χ' and χ'' were done on a commercial SQUID magnetometer using h_o=87.5 mA/m (7 Oe).

For two representative samples with size D=11.7 nm and D=21 nm, plots of experimental χ' and χ'' vs. T are shown in Figs. 3 and 4 respectively. Similar data were obtained for the other two samples. It is evident that T_B determined by the peak in χ'' increases with increase in f_m as predicted by Eqs. (6) and (7). Peaks in χ' are broad and occur at temperatures higher than that for χ'' in agreement with the prediction $\chi''=-(\pi/2)\partial(\ln\chi')/\partial\ln\omega$ [2].

Following Eq. (7), we show the plots of T_B vs. $1/\ln(f_o/f_m)$ for $f_o=2.6\times10^{10}$ Hz in Fig. 5 and in the inset for $f_o=2.6\times10^{9}$ Hz. We determined $f_o=2.6\times10^{10}$ Hz by first assuming $T_o=0$ and plotting $\ln f_m$ vs. $1/T_B$ with the intercept yielding $\ln f_o$ (Fig. 6). The magnitude of $f_o=2.6\times10^{9}$ Hz was estimated in earlier studies for the D≃4 nm Ni/SiO_2 system [7,12]. Both choices of f_o appear to give good linear fits in Fig. 5, although for the lower f_o, the magnitudes of T_o increases somewhat. For $f_o=2.6\times10^{10}$ Hz, the evaluated magnitudes of $T_a(T_o)$ are 320(0) K, 990(0) K, 1370(6) K and 1500(9) K for D=3.8 nm, 11.7 nm, 15 nm and 21nm, respectively. The zero magnitudes of T_o suggest the absence of IPI in the two smaller particles and the presence of weak IPI in the two larger particles because of non-zero T_B. This is further confirmed by the evaluation of the parameter $\Phi = \Delta T_B/[T_B\Delta\log_{10}f_m]$ which represents fractional change in T_B per decade change in f_m [13]. Experiments have shown that Φ is very small (0.005-0.05) for spin glasses and $\Phi\geq0.13$ for isolated NP [13]. For intermediate values ($0.005<\Phi<0.13$), IPI is present with its effect decreasing with increasing Φ. Determining ΔT_B for maximum and minimum f_m in our experiments, Φ=0.16, 0.13, 0.12 and 0.12 is found respectively for the D=3.8 nm, 11.7 nm, 15 nm and 21 nm samples. These magnitudes of Φ agree with our earlier conclusion of zero IPI in the two smaller NPs and a very weak IPI in the two large NPs. The presence of non-zero IPI is probably due to the larger moments on the larger NPs. Clearly, plots like those in Fig. 5 are essential to determine T_o if the magnitude of f_o is known, at least approximately.

Next, the magnitudes of $T_a=K_aV/k$ are used to determine the anisotropy constant K_a assuming spherical NPs. The computed values of K_a (in units of 10^4 J/m^3) are 15.4, 1.6, 1.1 and 0.4 respectively for the =3.8 nm, 11.7 nm, 15 nm and 21 nm samples. The observed increase in K_a with decreasing D has been reported and discussed in other systems also, the source being increasing surface anisotropy with decreasing D [3-6].

To test the validity of the correlation between χ'' and $\partial(\chi'T)/\partial T$ predicted by Eq. (8), the plots of the experimental χ'' and $\partial(\chi'T)/\partial T$ vs. T are shown in Fig. 7. All primary features of experimental χ'', such as the frequency and T dependence, are evident in the plots of $C\partial(\chi'T)/\partial T$, except that the peak magnitudes are off by a factor of about 2. This discrepancy is likely related to the approximations made in deriving the magnitude of C in Eq. (8) [2]. It may be relevant to note that in bulk antiferromagnets near the Néel temperature, $\partial(\chi'T)/\partial T$ is proportional to the specific heat [14].

The research at West Virginia University was supported in part by U. S. Department of Energy (Contract # DE- FC-26-05NT42456).

REFERENCES

1. L. Néel , Ann. Géophys. 5, 99 (1949).

2. L. Lundgren, P. Svedlindh and O. Beckman, J. Magn. Magn. Mater. 25, 33 (1981).

3. F. Bodkar, S. Morup and S. Linderoth, Phys. Rev. Lett. 72, 282 (1994).

4. K. Gilmore, Y. U. Idzerda, M. T. Klem, M. Allen, T. Douglas and M. Young, J. Appl. Phys. 97, 10B301 (2005).

5. R. Yanes, O. C. Fesenko, H. Kachkachi, D. A. Garanin, R. Evans and R. W. Chantrell, Phys. Rev.B 76, 064416 (2007).

6. H. Shim, P. Dutta, M. S. Seehra and J. Bonevich, Solid St. Commun. 145, 192 (2008).

7. V. Singh, M. S. Seehra and J. Bonevich, J. Appl. Phys. 103, 07D524 (2008).

8. J. -O. Andersson, C. Djurberg, T. Jonsson, P. Svedlindh and P. Nordblad, Phys. Rev.B 56, 13983 (2004).

9. S. Shtrikman and E. P. Wohlfarth, Phys. Lett. 85A, 467 (1981).

10. J. L. Tholence, Solid St. Commun. 88, 917 (1993).

11. H. Shim, A. Mannivannan, M. S. Seehra, K. M. Reddy and A. Punnoose, J. Appl. Phys. 99, 08Q503 (2006).

12. G. F. Goya, F. C. Fonseca, R. F. Jardim, R. Muccillo, N. L. V. Carreno, E. Longo and E. R. Leite, J. Appl. Phys. 93, 6531 (2003).

13. J. L. Dormann, L Bessais, and D. Fiorani, J. Phys. C: Solid State Phys, 21, 2015 (1988).

14. E. E. Bragg and M. S. Seehra, Phys. Rev. B, 7, 4197 (1973); M. E. Fisher, Philos Mag., 7, 1731 (1962).

FIGURE CAPTIONS

Fig. 1 Inset shows the TEM micrograph for the D=21 nm sample. The solid line is a fit to the log-normal distribution of the histogram of particle sizes.

Fig. 2 Room temperature XRD patterns of the four samples with the Miller indices of lines due to FCC Ni shown.

Fig. 3 χ' and χ'' vs. T for D=11.7 nm at five frequencies shown.

Fig. 4 Same as in Fig. 3 except for the D=21 nm sample.

Fig. 5 Plots of T_B vs. $1/\ln(f_o/f_m)$ following Eq. (7) for $f_o=2.6\times10^{10}$ Hz. The inset shows similar plot for $f_o=2.6\times10^9$ Hz. The lines through the points are least-squares fits.

Fig. 6 Plots of $\ln f_m$ against T_B^{-1} to determine f_o and T_a from the Eq. $f_m = f_o\exp(-T_a/T_B)$. This equation assumes zero IPI (T_o=0). Although fits are good, the evaluated Ta values are somewhat higher that those determined in Fig. 5 (see text).

Fig. 7 Plots of experimental χ'' vs. T and computed $C\partial(\chi'T)/\partial T$ of Eq. (7) using the data of the D=21 nm sample.

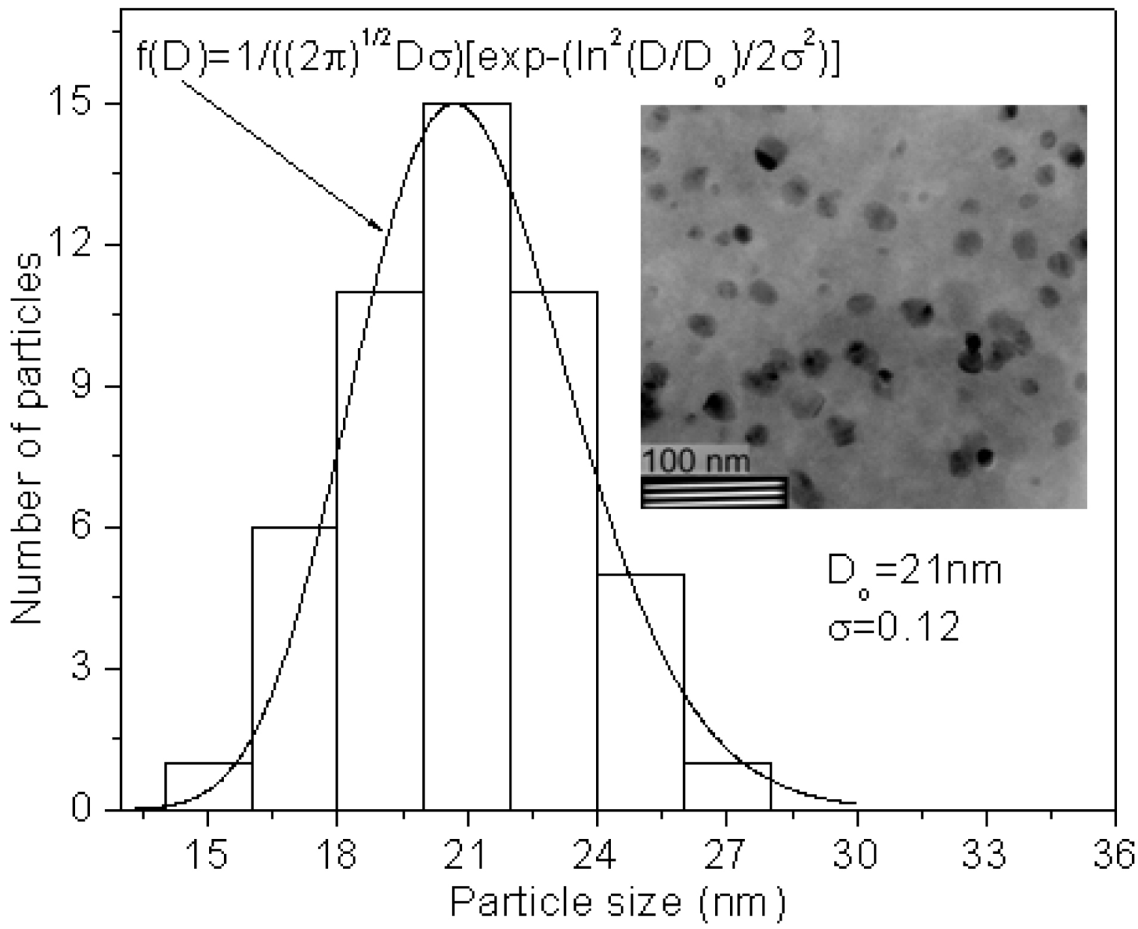

f(D)=1/((2π)^1/2 Dσ)[exp-(ln^2(D/D_o)/2σ^2)]
Number of particles
Particle size (nm)
0
3
6
9
12
15
15
18
21
24
27
30
33
36
100 nm
D_o=21nm
σ=0.12

Figure 1

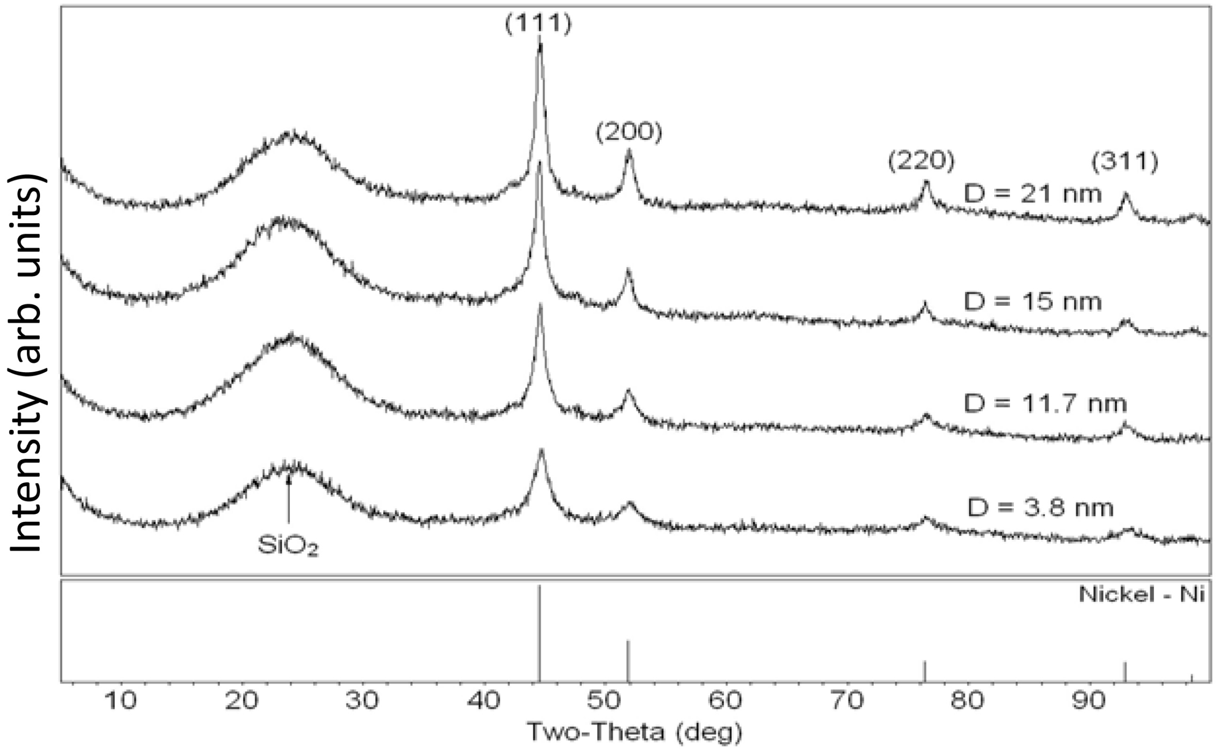
(111)
(200)
(220)
(311)
D = 21 nm
D = 15 nm
D = 11.7 nm
D = 3.8 nm
Intensity (arb. units)
SiO2
Nickel - Ni
10
20
30
40
50
60
70
80
90
Two-Theta (deg)

Figure 2

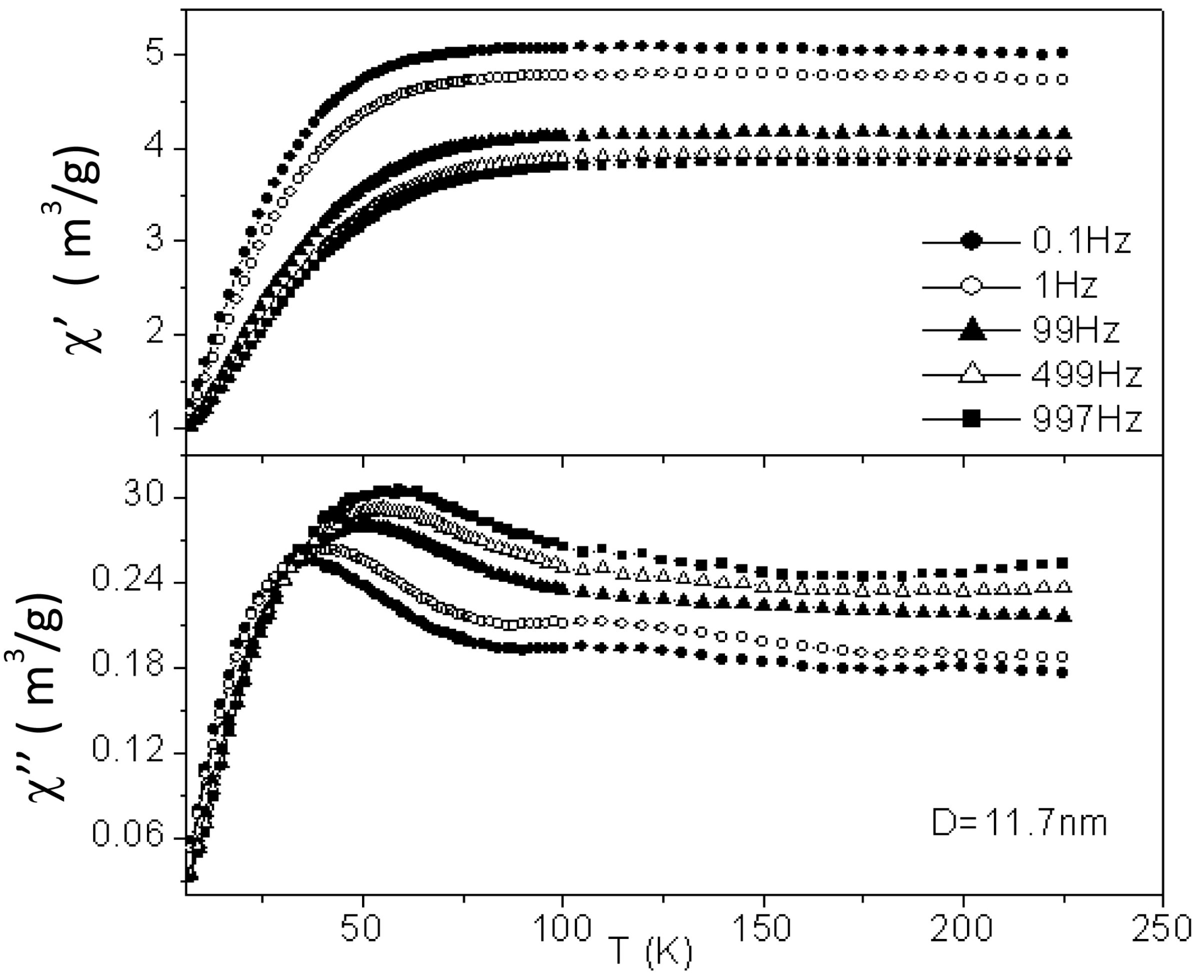

5
4
3
2
1
χ' (m^3/g)
0.1Hz
1Hz
99Hz
499Hz
997Hz
30
0.24
0.18
0.12
0.06
χ'' (m^3/g)
D= 11.7nm
50
100
150
200
250
T (K)

Figure 3

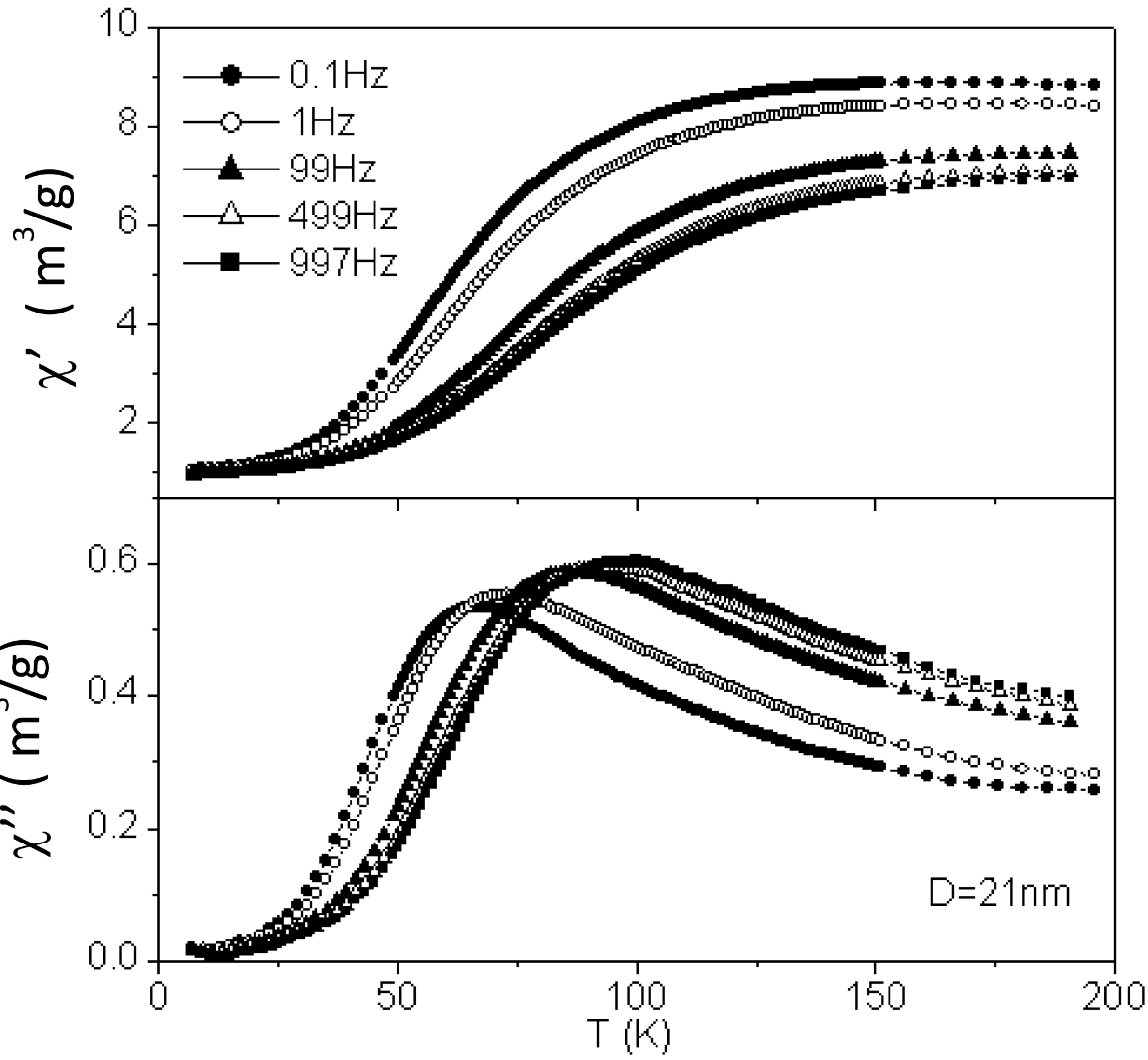

Figure 4.

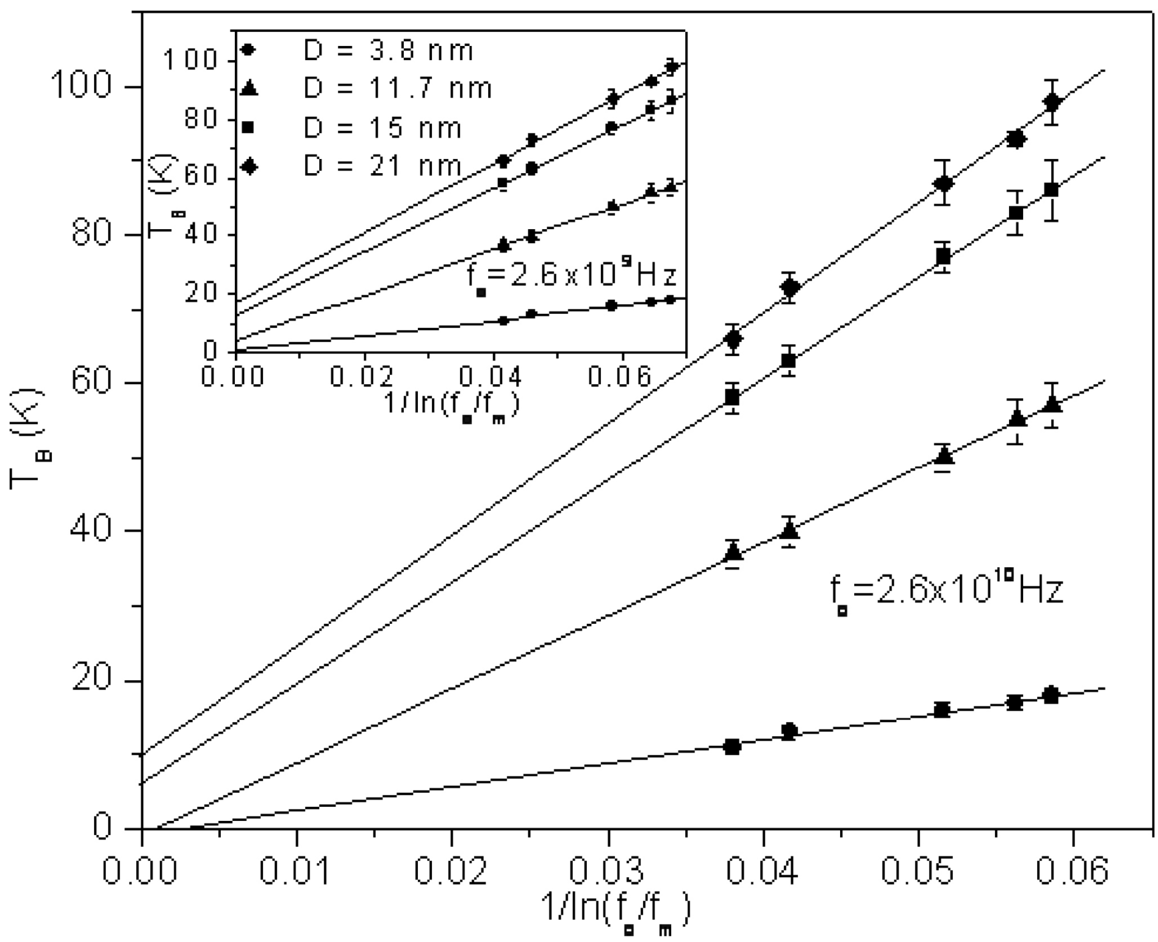

D = 3.8 nm
D = 11.7 nm
D = 15 nm
D = 21 nm
f_o=2.6x10^{9}Hz
1/ln(f_o/f_m)
T_B (K)
f_o=2.6x10^{10}Hz

Figure 5

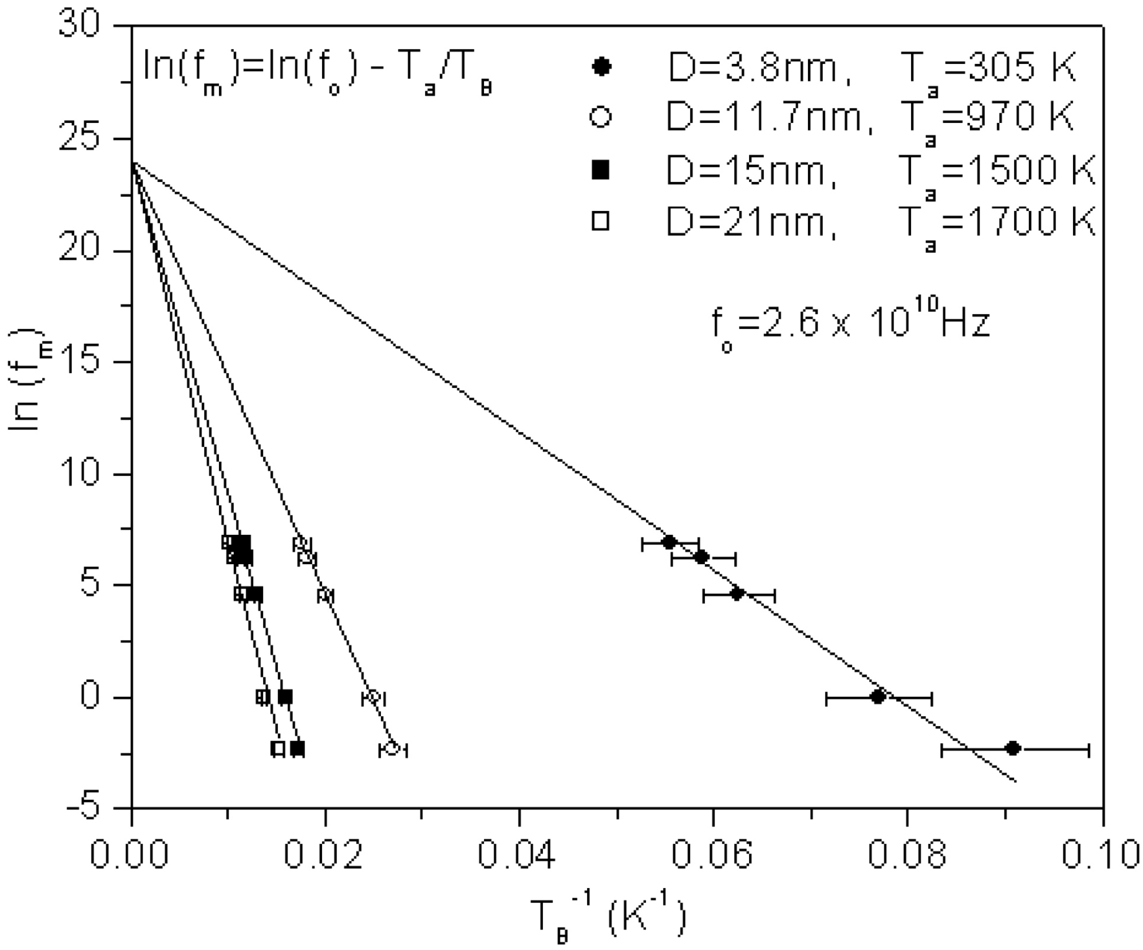
ln(f_m)=ln(f_o) - T_a/T_B
D=3.8nm, T_a=305 K
D=11.7nm, T_a=970 K
D=15nm, T_a=1500 K
D=21nm, T_a=1700 K
f_o=2.6 x 10^10 Hz
ln (f_m)
T_B^-1 (K^-1)
30
25
20
15
10
5
0
-5
0.00
0.02
0.04
0.06
0.08
0.10

Figure 6

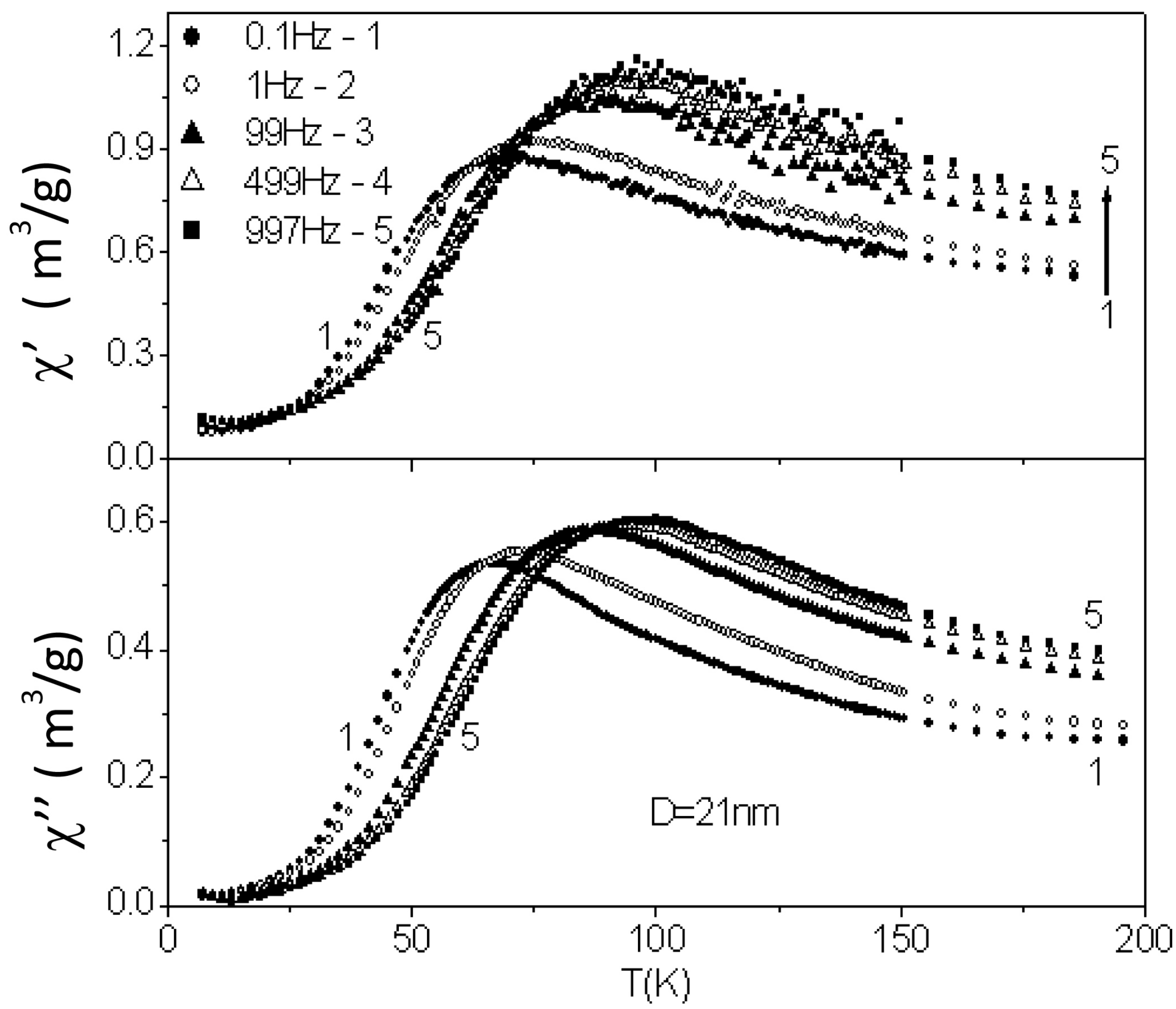
0.1Hz - 1
1Hz - 2
99Hz - 3
499Hz - 4
997Hz - 5
χ' (m3/g)
χ'' (m3/g)
D=21nm
T(K)
0.0
0.3
0.6
0.9
1.2
0.0
0.2
0.4
0.6
0
50
100
150
200
1
5

Figure 7